

## **MOVING COORDINATE FRAME FDTD ANALYSIS OF LONG RANGE TRACKING OF PULSED FIELDS IN GRADED INDEX WAVEGUIDES**

Y. Pemper, V. Lomakin, E. Heyman, and R. Kastner

Department of Electrical Engineering  
–Physical Electronics  
Tel-Aviv University  
Tel-Aviv 69978, Israel

R. W. Ziolkowski

Department of Electrical and Computer Engineering  
University of Arizona  
Tucson, AZ 85721, USA

- 1. Introduction**
  - 2. The Moving Coordinate Frame FDTD Code**
    - 2.1 Field Equations in the Moving Coordinate Frame
    - 2.2 Numerical Dispersion
    - 2.3 Numerical Stability
    - 2.4 Absorbing Boundary Conditions
      - 2.4.1 *ABC's for the Back and Front Boundaries Using the Diagonalization Approach*
      - 2.4.2 *Side Boundary*
      - 2.4.3 *Corner Points*
  - 3. Numerical Examples: Pulsed Beams in Nonuniform Quadratic Guides**
    - 3.1 Physical Configuration
    - 3.2 Numerical Results
  - 4. Summary and Conclusions**
- Appendices**  
**References**

## 1. INTRODUCTION

With the increase in the bandwidth of radiation and detection hardware, there is an ever-increasing interest in the propagation of ultrafast pulses in complex linear and nonlinear environments. A major challenge encountered in the course of development of this technology is the modeling of the propagation of pulsed fields over large distances using an explicit, discrete numerical approach such as the conventional FDTD scheme [1–3]. The major difficulties are the vast computer resources needed to discretize the entire region of interest and the accumulation of numerical dispersion errors, which may affect significantly the results for very long range propagation.

The moving coordinate frame FDTD approach makes tracking of the wavepacket field over long distances feasible because (a) instead of modeling a very large computational space with a stationary coordinate frame, the numerical effort is confined to the restricted region containing the pulse, (b) the space-time trajectory for the moving frame is calculated analytically using ray techniques, and (c) numerical dispersion errors are significantly reduced since the pulse is almost stationary in the moving frame, once frame speed has been analytically determined as the physical speed of the center-of-mass of the pulse. The method was initially presented for the inhomogeneous one dimensional case in [4–5], while a similar one-dimensional moving frame FDTD formulation has been used in [6] for pulse propagation in a homogeneous, nonlinear optical medium. A related paper addresses the application of this approach to the three-dimensional problem of long range tracking of collimated wavepackets [7].

Moving frame concepts have been used extensively in various analytical and numerical techniques in the past, mostly in the form of the frequency domain parabolic equation (PE) method which is also termed in the optical context as the beam propagation method (BPM) [8, 9 (Ch. 6), 10–12]. These methods have also been extended to the time-domain parabolic equation (TDPE) method [13, 9 (Ch. 8)]. They are based on the extraction of the rapidly varying part of the solution, which is known analytically, resulting in an approximate, one-way (parabolic type) equation for the slowly varying term. This approach is very robust and has been used extensively for long range tracking of wave fields in complex media. It suffers, however, from several drawbacks, i.e., the one-way approximation *a priori* precludes interactions which produce backward-propagating solutions, it assumes weak

inhomogeneities and a limited propagation angle.

The moving frame FDTD method is free of these limitations. It is general, robust and fully vectorial, with no limitations on the medium inhomogeneity. It is not based on the one-way approximation and thus provides a full wave solution. Furthermore, the inhomogeneity in the  $z$  direction is treated by mapping the  $z$  axis into an optical length coordinate (see (4)), which lends itself naturally to the description of fields in inhomogeneous media.

As mentioned above, we have recently applied the method for the three-dimensional problem of long range tracking of collimated wave-packets [7]. Here we address the electromagnetic/optical waveguide problem of long range tracking of cylindrically symmetric pulsed fields propagating along a waveguiding structure such as an optical fiber. In order to describe the method in the most transparent fashion, we refer to a vector acoustic equivalent of the problem which possesses fewer vector components than its electromagnetic counterpart. Yet the results are directly applicable to electromagnetic, or other, wave fields.

The waveguiding structures considered are characterized by monotonic increase of the wavespeed away from their axes (like a graded index optical fiber). Our code also accommodates inhomogeneities *along* the waveguide axis. The moving frame FDTD code for cylindrically symmetric configurations is presented in Section 2. In order to account correctly for the physical propagation speed of the pulsed guided modes, the coordinate frame speed is chosen as the local wavespeed along the axis. The numerical dispersion and stability expressions, are then derived in Sections 2.2 and 2.3, respectively. The absorbing boundary conditions (ABC's) (Section 2.4) are, in essence, adaptations of the first order Engquist-Majda-Mur [14–15] conditions. The difficulty in the moving frame formulation is that the forward propagating wave constituents are essentially stationary within the moving frame. This introduces certain peculiarities into the ABC's at the front and back faces since the forward propagating constituents are also stationary with respect to these faces and therefore cannot be removed.

The scheme developed in Section 2 is applied in Section 3 to solve pulse propagation along a waveguiding structure with a quadratic profile. The initial field distributions are taken to be of a pulsed beam (PB) type [16]: such solutions maintain their wavepacket structure over a considerable distance along the guide. Approximate time-domain

expressions for these fields in uniform and non-uniform guides, describing the wavepacket dynamics, are developed in Appendix A.1 using the techniques in [16]. For the longitudinally uniform guide, the results of the FDTD solution are also compared with exact frequency-domain modal solution [17], while for a longitudinally nonuniform guide we developed in Appendix A.2 an adiabatic type modal solution. The numerical solution which is obtained successfully recovers the field even at large distances and accommodates the physical (as opposed to numerical) dispersion characteristics of the modal solution. This and other conclusions are summarized in Section 4.

## 2. THE MOVING COORDINATE FRAME FDTD CODE

### 2.1 A Field Equations in the Moving Coordinate Frame

As has been mentioned in the Introduction, we will present the moving frame FDTD in the context of the vector acoustic field; however the results are directly applicable to the vector electromagnetic case. We consider the acoustic wave equations

$$\partial_t \mathbf{v} = -\frac{1}{\rho} \nabla p \quad \partial_t p = -c^2 \rho \nabla \cdot \mathbf{v}, \quad (1)$$

where  $p$  is the pressure,  $\mathbf{v}$  is the particle velocity vector,  $\rho = \rho(\mathbf{x})$  and  $c = c(\mathbf{x})$  are the density and sound speed of the medium, respectively and  $\mathbf{x} = (x, y, z)$  denotes the position in a 3D coordinate frame. We shall assume here that  $\rho = 1$ , while  $c$  has the cylindrically symmetric form

$$c = c(z, r), \quad r = \sqrt{x^2 + y^2} \quad (2)$$

with a *minimum* on the  $z$  axis and a monotonically increasing profile away from the  $z$  axis. This structure can support guided waves that propagate along the  $z$  axis. Since the propagation speed of these waves is close to the axial speed, we denote the axial sound speed by the special symbol

$$\bar{c}(z) \equiv c(r, z)|_{r=0}, \quad (3)$$

and introduce the moving coordinate frame variable  $\zeta$  via

$$\zeta = \int_0^z \frac{c_0}{\bar{c}(z')} dz' - c_0 t, \quad (4)$$

where  $c_0$  is an arbitrary reference velocity. The integral in (4) defines the “optical” path length that maps the  $z$  axis onto an equi-propagation-time axis. Subtracting  $c_0 t$  renders  $\zeta$  an optical coordinate centered around the pulse’s center of mass.

We now transform the field equations into the moving frame. To this end, we denote

$$\mathbf{v}(x, y, z, t) = \hat{\mathbf{z}}V(x, y, \zeta, t) + \mathbf{U}(x, y, \zeta, t), \quad \text{where } \mathbf{U} \cdot \hat{\mathbf{z}} = 0 \quad (5a)$$

$$p(x, y, z, t) = P(x, y, \zeta, t), \quad (5b)$$

where here and henceforth we use a caret to denote unit vectors. For mathematical convenience we have also separated the longitudinal and transversal components of the particle velocity vector, denoting them as  $V$  and  $\mathbf{U}$ , respectively. Using (4), the stationary field equations (1) are transformed into the moving frame, as follows:

$$\partial_t V = c_0 \partial_\zeta V - \frac{c_0}{\tilde{c}} \partial_\zeta P \quad (6a)$$

$$\partial_t \mathbf{U} = c_0 \partial_\zeta \mathbf{U} - \nabla_t P \quad (6b)$$

$$\partial_t P = c_0 \partial_\zeta P - \frac{c_0 \tilde{c}^2}{\tilde{c}} \partial_\zeta V - \tilde{c}^2 \nabla_t \cdot \mathbf{U}, \quad (6c)$$

where  $\nabla_t = \hat{\mathbf{x}}\partial_x + \hat{\mathbf{y}}\partial_y$  and we also use the tilde to denote velocities in the moving frame, i.e.,  $\tilde{c}(\zeta, r, t) = c[z(\zeta, t), r]$  and  $\tilde{c}(\zeta, t) = \bar{c}[z(\zeta, t)]$ .

In this article we shall only consider cylindrically symmetric wave solutions, thereby reducing the size of the problem. Accordingly, we denote  $\mathbf{U} = \hat{\mathbf{r}}U$ , bringing (6) to the form

$$\partial_t V = c_0 \partial_\zeta V - \frac{c_0}{\tilde{c}} \partial_\zeta P \quad (7a)$$

$$\partial_t U = c_0 \partial_\zeta U - \partial_r P \quad (7b)$$

$$\partial_t P = c_0 \partial_\zeta P - \frac{c_0 \tilde{c}^2}{\tilde{c}} \partial_\zeta V - \tilde{c}^2 \frac{1}{r} \partial_r(rU), \quad (7c)$$

with the axial boundary conditions  $\partial_r P = \partial_r V = U = 0$  at  $r = 0$ .

The central-difference discretized form of (7), organized in a “marching in time” form, is thus:

$$V_{i,j}^{n+1} = V_{i,j}^{n-1} + \gamma_\zeta (V_{i+1,j}^n - V_{i-1,j}^n) - (\gamma_\zeta / \tilde{c}_i^n) (P_{i+1,j}^n - P_{i-1,j}^n) \quad (8a)$$

$$U_{i,j}^{n+1} = U_{i,j}^{n-1} + \gamma_\zeta (U_{i+1,j}^n - U_{i-1,j}^n) - (\gamma_r / c_0) (P_{i,j+1}^n - P_{i,j-1}^n) \quad (8b)$$

$$P_{i,j}^{n+1} = P_{i,j}^{n-1} + \gamma_\zeta (P_{i+1,j}^n - P_{i-1,j}^n) - (\gamma_\zeta (\tilde{c}_{i,j}^n)^2 / \tilde{c}_i^n) (V_{i+1,j}^n - V_{i-1,j}^n) \\ - (\gamma_r (\tilde{c}_{i,j}^n)^2 / c_0) \frac{1}{r_j} (r_{j+1} U_{i,j+1}^n - r_{j-1} U_{i,j-1}^n). \quad (8c)$$

The problem space is discretized uniformly:  $t$ ,  $\zeta$  and  $r$  are sampled at the points  $t_n = n\Delta t$ ,  $\zeta_i = i\Delta\zeta$ ,  $r_j = j\Delta r$ , where  $i = 0, 1, \dots, I$  and  $j = 0, 1, \dots, J$  [1]. We denote  $\gamma_\zeta = \frac{c_0\Delta t}{\Delta\zeta}$ ,  $\gamma_r = \frac{c_0\Delta t}{\Delta r}$ ,  $\tilde{c}_{i,j}^n = \tilde{c}(i\Delta\zeta, j\Delta r, n\Delta t)$ , and  $\tilde{c}_i^n = \tilde{c}(i\Delta\zeta, n\Delta t)$ .

The singularity of Eq. (8c) at  $r = 0$  requires a special treatment. Note that Eq. (8a) applies for  $j \geq 0$ , while (8b) and (8c) apply for  $j \geq 1$ . In (8b) we have  $U = 0$  for  $j = 0$ . The singularity of (8c) at  $r = 0$  is addressed by integrating (7c) within the elementary volume  $dv = 2\pi r dr d\zeta$  around the  $r = 0$  axis. Following essentially the same procedure outlined in [7, Eqs. (8)–(11)] we obtain

$$\begin{aligned} P_{i,0}^{n+1} &= P_{i,0}^{n-1} + \gamma_\zeta(P_{i+1,0}^n - P_{i-1,0}^n) \\ &\quad - \tilde{c}_i^n \gamma_\zeta (V_{i+1,0}^n - V_{i-1,0}^n) - 4(\tilde{c}_i^n)^2 c_0^{-1} \gamma_r U_{i,1}^n. \end{aligned} \quad (9)$$

which replaces (8c) for  $j = 0$ .

## 2.2 Numerical Dispersion

In order to derive the numerical dispersion relation, we may assume in the analysis that the medium is locally uniform in the  $z$  direction so that the sound speed has the form  $\bar{c}/\bar{n}(r)$ , where, again, we point out that  $\bar{n} = 1$  on the axis and decreases monotonically away from it. We make an ansatz for a space-time harmonic solution of the following form:

$$\begin{pmatrix} V_{i,j}^n \\ U_{i,j}^n \\ P_{i,j}^n \end{pmatrix} = \begin{pmatrix} V_0 J_0(k_r r_j) \\ U_0 J_1(k_r r_j) \\ P_0 J_0(k_r r_j) \end{pmatrix} e^{-i[\omega t_n - k_\zeta \zeta_i]} \quad (10)$$

where  $k_r$  and  $k_\zeta$ , are wave numbers;  $J_0$  and  $J_1$  are Bessel functions of the zero and first order, respectively. We denote  $\iota = \sqrt{-1}$ , in order to avoid confusion with the subscript  $i$ . Substituting (10) into (8), we obtain the matrix equation

$$\begin{pmatrix} \sin \Omega + \gamma_\zeta \sin K_\zeta & 0 & -\gamma_\zeta \bar{c}^{-1} \sin K_\zeta \\ 0 & \sin \Omega + \gamma_\zeta \sin K_\zeta & -\iota \gamma_r c_0^{-1} K_r \\ -\gamma_\zeta \bar{c} \bar{n}_j^{-2} \sin K_\zeta & \iota \gamma_r \bar{c}^2 c_0^{-1} \bar{n}_j^{-2} K_r & \sin \Omega + \gamma_\zeta \sin K_\zeta \end{pmatrix} \begin{pmatrix} V_0 \\ U_0 \\ P_0 \end{pmatrix} = 0 \quad (11)$$

where  $K_\zeta = k_\zeta \Delta\zeta$ ,  $K_r = k_r \Delta r$ ,  $\Omega = \omega \Delta t$  and  $\bar{n}_j = \bar{n}(j\Delta r)$ . The local numerical dispersion relation is derived from the zeros of the determinant:

$$\sin \Omega + \gamma_\zeta \sin K_\zeta = 0 \quad (12a)$$

$$(\sin \Omega + \gamma_\zeta \sin K_\zeta)^2 - \frac{1}{\bar{n}_j^2} \gamma_\zeta^2 \sin^2 K_\zeta - \frac{\bar{c}^2}{c_0^2 \bar{n}_j^2} \gamma_r^2 K_r^2 = 0. \quad (12b)$$

Eq. (12a) describes backward propagation at a wavespeed close to  $-c_o$  in the moving frame, corresponding, in the stationary frame, to a radial propagation (cf. [7, Eq. (14a)]). Eq. (12b) resembles Eq. (14b) in [7]; however, it has some important differences due to the transversal inhomogeneity. Following [7, Eq. (16)] it may be rewritten as

$$\begin{aligned} \sin \Omega + \gamma_\zeta \sin K_\zeta &= \pm \bar{n}_j^{-1} \gamma_\zeta \sin K_\zeta \sqrt{1 + \frac{\bar{c}^2 \gamma_r^2}{c_0^2 \gamma_\zeta^2} \frac{K_r^2}{\sin^2 K_\zeta}} \\ &\approx \pm \bar{n}_j^{-1} \gamma_\zeta \sin K_\zeta \sqrt{1 + \frac{\bar{c}^2 k_r^2}{c_0^2 k_\zeta^2}}, \end{aligned} \quad (13)$$

where the approximation applies for small  $K_\zeta$ . We approximate the resulting numerical dispersion assuming an excitation by collimated fields, characterized by

$$(k_r/k_\zeta)^2 \equiv \epsilon \ll 1. \quad (14)$$

Using (14), Eq. (13) reduces to

$$\sin \Omega \approx \left( -1 \pm \bar{n}_j^{-1} \pm \frac{1}{2} \epsilon \bar{n}_j^{-1} \bar{c}^2 / c_0^2 \right) \gamma_\zeta \sin K_\zeta. \quad (15)$$

The upper sign is related to the forward propagating spectra, giving, for small  $\Omega$  and  $K_\zeta$

$$v_p = \frac{\omega}{k_\zeta} \approx c_0 \left( \bar{n}_j^{-1} - 1 + \frac{1}{2} \epsilon \bar{n}_j^{-1} \bar{c}^2 / c_0^2 \right) \quad (16)$$

For the collimated field, (16) implies  $v_p \ll c_0$ , i.e., the wave is practically stationary, in regions close to the axis. Note, however, that unlike the plane stratified medium case of [7], the wave is not quite stationary in regions away from the axis, where  $\bar{n}_j < 1$ , but is rather forward propagating due to the faster off-axis sound speed.

The lower sign in (15) pertains to the backward propagating constituents. It gives, for small  $\Omega$  and  $K_\zeta$ ,

$$v_p = \frac{\omega}{k_\zeta} \approx -c_0 \left( \bar{n}_j^{-1} + 1 + \frac{1}{2} \epsilon \bar{n}_j^{-1} \bar{c}^2 / c_0^2 \right), \quad (17)$$

such that  $v_p \approx -2c_0$  on axis.

### 2.3 Numerical Stability

To determine the stability condition, we first substitute  $g = e^{-i\Omega}$  into the numerical dispersion relations (12):

$$g^{-1} - g + i2\gamma_\zeta \sin K_\zeta = 0, \quad (18a)$$

$$(g^{-1} - g + i2\gamma_\zeta \sin K_\zeta)^2 + 4(\bar{c}/c_0)^2 \bar{n}_j^{-2} \gamma_r^2 K_r^2 + 4\bar{n}_j^{-2} \gamma_\zeta^2 \sin^2 K_\zeta = 0. \quad (18b)$$

Stability requires that  $gg^* \leq 1 \forall$  real  $K_\zeta$  and  $K_r$ . Imposing this condition on (18a) yields the first stability criterion

$$\gamma_\zeta \leq 1, \quad (\text{i.e., } c_0 \Delta t \leq \Delta \zeta). \quad (19)$$

Next, to determine the stability condition implied by (18b), we first rewrite it in the form

$$g^2 - i2g\gamma_\zeta \sin K_\zeta \left( 1 \pm \bar{n}_j^{-1} \sqrt{1 + \epsilon \bar{c}^2 / c_0^2} \right) - 1 = 0, \quad (20)$$

where we have used the same approximation as in (13)–(14). The solutions of (20) satisfy  $|g_1||g_2| = 1$ , implying  $|g_1| = |g_2| = 1$ . Since this condition should be satisfied  $\forall K_z, K_r$ , the stability condition becomes

$$\gamma_\zeta^2 \left( 1 \pm \bar{n}_j^{-1} \sqrt{1 + \epsilon \bar{c}^2 / c_0^2} \right)^2 \leq 1. \quad (21)$$

Taking the upper sign in (21), we obtain  $\gamma_\zeta \leq \left( 1 + \bar{n}_j^{-1} \sqrt{1 + \frac{1}{2} \epsilon \bar{c}^2 / c_0^2} \right)^{-1} \approx \frac{\bar{n}_j}{1 + \bar{n}_j} \leq \frac{\bar{n}_J}{1 + \bar{n}_J}$ , where the latter condition is obtained by noting that  $\bar{n}(r)$  is monotonically decreasing away from the center. Generalizing this condition for non-uniform guides we replace  $\bar{n}_J$  by  $\bar{n}_J(z) = \bar{c}(z)/c(r_{\max}, z)$ , resulting in

$$\gamma_\zeta \leq \min_z \left\{ \frac{\bar{n}_J(z)}{1 + \bar{n}_J(z)} \right\} = \min_z \left\{ \frac{\bar{c}(z)}{\bar{c}(z) + c(r_{\max}, z)} \right\}. \quad (22)$$

The stability condition (22) is stronger than (19), because it is related to the back-propagating wave for which  $v_p \approx -2c_0$ , whereas (22) matches the radially propagating wave. This strong condition

will be used throughout. It is the analog of the CFL condition in the stationary coordinate frame, recalling that in the moving coordinate frame the greatest wave speed is that of the backward propagating wave at off-axis points, and it is given by  $c_0\left(1 + \frac{c(r_{\max}, z)}{\tilde{c}(z)}\right)$ . Taking, on the other hand, the lower sign in (21), we obtain

$$\gamma_\zeta \leq \left| 1 - \bar{n}_j^{-1} \sqrt{1 + \epsilon \tilde{c}^2 / c_0^2} \right|^{-1} \approx \frac{\bar{n}_j}{1 - \bar{n}_j}. \quad (23)$$

This condition is much weaker than (22), and therefore will not be used. It is related to the forward propagating wave, which is almost stationary. Therefore, this condition places no practical limit on  $\gamma_\zeta$ .

## 2.4 Absorbing Boundary Conditions

The formulation of boundary conditions for the moving coordinate frame is now addressed. We assume, without loss of generality, that our grid is located in the region between  $0 \leq \zeta \leq \zeta_{\max}$  and  $0 \leq r \leq r_{\max}$ .

### 2.4.1 ABC's for the Back and Front Boundaries Using the Diagonalization Approach

In general, first order boundary conditions are found by considering local propagation in a direction normal to the boundary at hand. Consequently, when considering the back boundary  $\zeta = 0$  and the front boundary  $\zeta = \zeta_{\max}$ , we assume  $\partial_r = 0$  in (7), obtaining:

$$\partial_t V = c_0 \partial_\zeta V - \frac{c_0}{\tilde{c}} \partial_\zeta P \quad (24a)$$

$$\partial_t U = c_0 \partial_\zeta U \quad (24b)$$

$$\partial_t P = c_0 \partial_\zeta P - \frac{c_0 \tilde{c}^2}{\tilde{c}} \partial_\zeta V. \quad (24c)$$

Next, in order to derive a boundary condition scheme that adapts to the local changes in the medium properties, we transform the relevant field constituents to adiabatic-type constituents

$$\tilde{P} = \tilde{c}^{-1/2} P, \quad \tilde{V} = \tilde{c}^{1/2} V, \quad (25)$$

thus obtaining from (24a) and (24c)

$$\partial_t \tilde{V} = c_0 \partial_\zeta \tilde{V} - c_0 \frac{\tilde{c}}{\tilde{c}} \partial_\zeta \tilde{P} - \frac{1}{2} \tilde{c}_z \tilde{P} \quad (26a)$$

$$\partial_t \tilde{P} = c_0 \partial_\zeta \tilde{P} - c_0 \frac{\tilde{c}}{\tilde{c}} \partial_\zeta \tilde{V} + \frac{1}{2} \tilde{c}_z \tilde{V}, \quad (26b)$$

where  $\tilde{c}_z(\zeta, r, t) \equiv \partial_z c(z, r)|_{z=z(\zeta, t)}$ . In deriving (26) we also note that  $c$  is  $t$ -independent so that  $(\partial_t - c_0 \partial_\zeta) \tilde{c}(\zeta, r, t) = 0$ . Adding and subtracting (26a) and (26b), one obtains

$$\partial_t \overset{\pm}{W} = c_0 \left( 1 - \frac{\tilde{c}}{\bar{c}} \right) \partial_\zeta \overset{\pm}{W} - \frac{1}{2} \tilde{c}_z \bar{W} \quad (27a)$$

$$\partial_t \bar{W} = c_0 \left( 1 + \frac{\tilde{c}}{\bar{c}} \right) \partial_\zeta \bar{W} + \frac{1}{2} \tilde{c}_z \overset{\pm}{W}, \quad (27b)$$

where

$$\overset{\pm}{W} = \tilde{P} \pm \tilde{V} = \tilde{c}^{-1/2} P \pm \tilde{c}^{1/2} V. \quad (28)$$

Neglecting the coupling terms, we finally obtain the diagonalized system of equations

$$\partial_t \overset{\pm}{W} = c_0 \left( 1 - \frac{\tilde{c}}{\bar{c}} \right) \partial_\zeta \overset{\pm}{W} \quad (29a)$$

$$\partial_t \bar{W} = c_0 \left( 1 + \frac{\tilde{c}}{\bar{c}} \right) \partial_\zeta \bar{W} \quad (29b)$$

$$\partial_t U = c_0 \partial_\zeta U. \quad (29c)$$

From (29), we readily recognize that  $\overset{\pm}{W}$ ,  $\bar{W}$ , and  $U$  satisfy the corresponding first-order one-way wave equations and propagate at velocities  $c_0 \left( \frac{\tilde{c}}{\bar{c}} - 1 \right)$ ,  $-c_0 \left( \frac{\tilde{c}}{\bar{c}} + 1 \right)$ , and  $-c_0$ , respectively, in the  $\zeta$  direction.

**The back boundary:** At the back boundary  $\zeta = 0$ ,  $\bar{W}$  is the incident one-way wave constituent and  $\overset{\pm}{W}$  is the one-way wave constituent which is reflected back into the numerical grid. Following a procedure introduced in [7], we may remove  $\overset{\pm}{W}$  from the problem space by letting it propagate at an arbitrary speed  $c_1$ . The effect of  $c_1$  on the numerical results has also been explored in [7]. Here we shall simplify the general formulation and choose  $c_1$  to be the speed at which  $\bar{W}$  is incident upon the back boundary. Thus, the boundary condition satisfied by  $\overset{\pm}{W}$  at the back boundary is (cf. (29a))

$$\partial_t \overset{\pm}{W} = c_0 \left( 1 + \frac{\tilde{c}}{\bar{c}} \right) \partial_\zeta \overset{\pm}{W}. \quad (30)$$

Combining (30) with (29b), we rewrite the boundary conditions in terms of the field constituents

$$\partial_t(\tilde{c}^{1/2}V) = c_0 \left(1 + \frac{\tilde{c}}{\bar{c}}\right) \partial_\zeta(\tilde{c}^{1/2}V) \quad (31a)$$

$$\partial_t(\tilde{c}^{-1/2}P) = c_0 \left(1 + \frac{\tilde{c}}{\bar{c}}\right) \partial_\zeta(\tilde{c}^{-1/2}P). \quad (31b)$$

Turning now to  $U$ , we use (29c). These continuous boundary conditions are discretized as follows:

$$\begin{aligned} V_{0,j}^{n+1} = & \frac{1}{\sqrt{\tilde{c}_{0,j}^{n+1}}} \left[ \sqrt{\tilde{c}_{1,j}^n} V_{1,j}^n + \frac{c_0(1 + A_j^n)\Delta t - \Delta\zeta}{c_0(1 + A_j^n)\Delta t + \Delta\zeta} \right. \\ & \left. \times \left( \sqrt{\tilde{c}_{1,j}^{n+1}} V_{1,j}^{n+1} - \sqrt{\tilde{c}_{0,j}^n} V_{0,j}^n \right) \right] \end{aligned} \quad (32a)$$

$$\begin{aligned} P_{0,j}^{n+1} = & \sqrt{\tilde{c}_{0,j}^{n+1}} \left[ \frac{P_{1,j}^n}{\sqrt{\tilde{c}_{1,j}^n}} + \frac{c_0(1 + A_j^n)\Delta t - \Delta\zeta}{c_0(1 + A_j^n)\Delta t + \Delta\zeta} \right. \\ & \left. \times \left( \frac{P_{1,j}^{n+1}}{\sqrt{\tilde{c}_{1,j}^{n+1}}} - \frac{P_{0,j}^n}{\sqrt{\tilde{c}_{0,j}^n}} \right) \right] \end{aligned} \quad (32b)$$

$$U_{0,j}^{n+1} = U_{1,j}^n + \frac{c_0\Delta t - \Delta\zeta}{c_0\Delta t + \Delta\zeta} (U_{1,j}^{n+1} - U_{0,j}^n), \quad (32c)$$

where

$$A_j^n = \frac{\tilde{c}_{0,j}^n + \tilde{c}_{1,j}^n + \tilde{c}_{0,j}^{n+1} + \tilde{c}_{1,j}^{n+1}}{\tilde{c}_{0,j}^n + \tilde{c}_{1,j}^n + \tilde{c}_{0,j}^{n+1} + \tilde{c}_{1,j}^{n+1}}. \quad (33)$$

**The front boundary:** At the front boundary ( $\zeta = \zeta_{\max}$ )  $\bar{W}$  is the forward moving one-way wave constituent impinging upon the boundary, while  $\bar{W}$  is the reflected one-way wave constituent. Yet, if we try to remove  $\bar{W}$  from the problem space at any removal speed, the numerical scheme becomes unstable, (see [7]). Recalling the fact that the moving frame tracks the forward moving wave constituents, we assume a null field ahead of the frame. Consequently, we may specify

$$\bar{W}|_{\zeta=\zeta_{\max}} = 0. \quad (34)$$

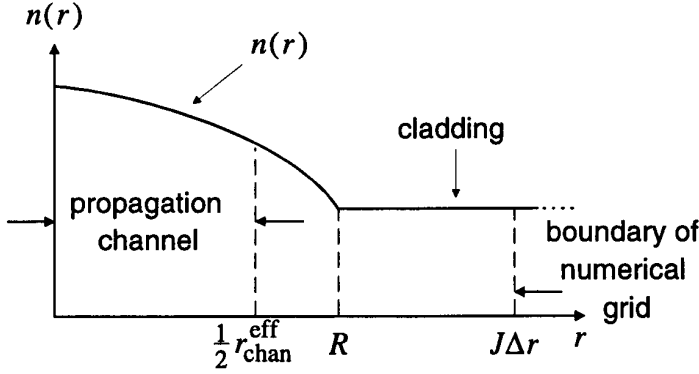


**Figure 1.** Profile of the graded index waveguide configuration. In the numerical simulation the waveguide has been surrounded with a constant  $n$  cladding region for  $r > R$ , where  $R$  has been chosen so that  $R \gg \frac{1}{2}r_{\text{chan}}^{\text{eff}}$ .

The same condition is used for  $U$ . Finally, for  $\overset{\dagger}{W}$  we use (29a). The numerical representation of these boundary conditions is

$$\overset{\dagger}{W}_{I,j}^{n+1} = \overset{\dagger}{W}_{I-1,j}^n + \frac{c_0(B_j^n - 1)\Delta t - \Delta\zeta}{c_0(B_j^n - 1)\Delta t + \Delta\zeta} \left( \overset{\dagger}{W}_{I-1,j}^{n+1} - \overset{\dagger}{W}_{I,j}^n \right) \quad (35a)$$

$$\bar{W}_{I,j}^{n+1} = 0 \quad (35b)$$

$$U_{I,j}^{n+1} = 0, \quad (35c)$$

where

$$B_j^n = \frac{\tilde{c}_{I,j}^n + \tilde{c}_{I-1,j}^n + \tilde{c}_{I,j}^{n+1} + \tilde{c}_{I-1,j}^{n+1}}{\tilde{c}_{I,j}^n + \tilde{c}_{I-1,j}^n + \tilde{c}_{I,j}^{n+1} + \tilde{c}_{I-1,j}^{n+1}}. \quad (36)$$

The final result for the actual field components is then

$$V_{I,j}^{n+1} = \frac{1}{2\sqrt{\tilde{c}_{I,j}^{n+1}}} \overset{\dagger}{W}_{I,j}^{n+1} \quad (37a)$$

$$P_{I,j}^{n+1} = \frac{\sqrt{\tilde{c}_{I,j}^{n+1}}}{2} \overset{\dagger}{W}_{I,j}^{n+1}. \quad (37b)$$

### 2.4.2 Side Boundary

A natural tendency for truncation of the grid in the  $r$  direction would be to use a Higdon-type operator as in [7]. However, attempting to use such an operator results in exponentially growing numerical solutions for large  $r$ , which, though being legitimate solutions of the wave equation outside of the propagation channel<sup>1</sup>, they are non-physical. To annul these solutions, we simulate the physical condition  $P, U \xrightarrow{r \rightarrow \infty} 0$ , by requiring a large enough numerical grid so that the boundaries are beyond the propagation channel, and then imposing the numerical boundary condition

$$P_{i,J}^{n+1} = 0, \quad U_{i,J}^{n+1} = 0 \quad (38)$$

For  $V$ , we use the field equation (8a) as before, since it has no derivatives in the  $r$  direction.

It should be noted, however, that extending the numerical grid to large  $r$  requires also a smaller time-step  $\Delta t$  as follows from the CFL condition in (22). To circumvent this problem we note that guided fields are exponentially decaying outside the propagation channel so that we may replace the medium at some distance beyond the effective propagation channel by a uniform cladding region shown in Fig. 1. Note also that even though the cladding region was introduced for numerical implementation reasons, the cladding geometry matches more closely real physical configurations.

### 2.4.3 Corner Points

At the corner points of the numerical grid boundary, we use the same approach as in [7]. At these points, both the  $\zeta$  direction and  $r$  direction boundary conditions apply. However, since the moving frame FDTD code is intended to track collimated pulsed fields that propagate mainly in the  $\zeta$  direction, we shall prefer the  $\zeta$  direction boundary conditions over the  $r$  direction ones and use the boundary conditions as given in Section 2.4.1.

---

<sup>1</sup> We use the term “propagation channel” to denote the region near the waveguide axis where the modal field is confined. Outside this region the physical solution is exponentially decaying. Note also that the propagation channel width typically increases as the frequency decreases (see Appendix A), and thus the “effective channel width” is approximated by the channel width at the lowest frequency  $\omega_{\min}$  in the signal.

### 3. NUMERICAL EXAMPLES: PULSED BEAMS IN NONUNIFORM QUADRATIC GUIDES

#### 3.1 Physical Configuration

We test the moving frame FDTD scheme on a quadratic profile waveguide having

$$c = \bar{c}(z)/\bar{n}(r), \quad \bar{n}(r, z) = \sqrt{1 - \nu^2(z)r^2} \quad (39)$$

We consider both longitudinally uniform guides with constant  $\bar{c}$  and  $\nu$ , for which an exact modal solution is available in the frequency domain, and nonuniform guides. Specifically we take  $\bar{c} = c_0(1 + az)$  with  $a = 0$  (uniform guide) or  $a = 0.015$  (slowly varying guide) and  $\nu = 7$ . The coordinates are chosen such that  $c_0 = 1$ . As indicated in Sec. 2.4.2, the guide is surrounded by a cladding region with constant  $\bar{n}$  for  $r > R$ , where  $R$  is chosen so that  $R \gg \frac{1}{2}r_{\text{chan}}^{\text{eff}}$ ,  $r_{\text{chan}}^{\text{eff}}$  being the effective propagation channel (see Fig. 1). For the quadratic guide, the channel width as a function of  $\omega$  is (see (A26a))  $r_{\text{chan}}(\omega) = \sqrt{8c_0/\nu\omega}$ , hence  $r_{\text{chan}}^{\text{eff}}$  is calculated by estimating  $\omega \approx T^{-1}$ , where  $T$  is the pulselength.

The initial field distributions are taken as those of the pulsed-beam (PB) type. Such fields maintain their wavepacket structure over a considerable propagation range. Furthermore, approximate time domain solutions are available for these cases (see Appendix. A.1). The initial data for the FDTD algorithm has thus been produced by setting  $t = 0$  in the wavepacket expression (A10), in which  $f^\dagger(t)$  is any analytic pulse (as defined in (A2)),  $q(z)$  and  $\alpha(z)$  are given in (A15) or in (A18) for a uniform or nonuniform guide, and  $\alpha(0)$  is a complex constant with  $\text{Im}\alpha(0) > 0$ . The properties of this wavepacket solution are discussed in detail in A.1. Here, we only mention the fact that the transversal confinement of the field is affected by the imaginary part of the argument in  $f^\dagger(t)$ , which becomes negative as  $r$  grows and thus causes a decay of the analytic signal. It should also be noted that the width of the PB fluctuates as it propagates in the guide (see discussion after (A15)), unless  $\alpha(0)$  is chosen as  $\alpha(0) = \nu(0)/\bar{c}(0)$ , in which case the PB is matched to the guide.

In our case, since the  $\bar{c}(z)$  changes slowly over the scale of the pulse length, we may calculate the initial data for the FDTD algorithm at  $t = 0$  and  $t = \Delta t$  by approximating the wavepacket expression (A10)

around  $z \approx 0$ , giving

$$\overset{+}{p}(\mathbf{r}, t) = \text{Re} \overset{+}{f}(t - z/\bar{c}(0) - \frac{1}{2}\alpha(0)r^2). \quad (40)$$

The excitation pulse in the numerical simulations has been chosen to be a twice differentiated analytic delta (or Lorentzian) pulse (see (A20))

$$\overset{+}{f}(t) = -\delta^{\dagger(2)}(t - i\frac{1}{2}T), \quad T > 0 \quad (41)$$

The parameter  $T$  that controls the pulse length has been taken to be  $c_0T = 1.410^{-2}$ .

### 3.2 Numerical Results

Numerical results for several test cases are shown in Figs. 2–4. “Matched” and “non-matched” PB initial conditions are shown in Figs. 2 and 3, respectively, for a uniform guide. The results are compared with the *exact* modal solution of Sec. A.2 (transformed into the time domain), and also with the approximate PB solution of Sec. A.1. Fig. 4 gives the corresponding results for a non-uniform guide with “non-matched” PB initial conditions. In this case the numerical results are compared with the adiabatic mode solution of Appendix A.2, and also with the PB solution of Appendix A.1.

The case represented by Fig. 2 corresponds to a uniform guide with  $\bar{c}(0) = \bar{c}_0 = 1$  and  $\nu(0) = \nu_0 = 7$  and PB initial conditions with  $\alpha(0) = i7 = i\nu(0)/\bar{c}(0)$ . In this case the PB is matched to the guide and the exact solution is described by a single mode as discussed after (A33): The reference mode solution has been calculated by numerically transforming into the time domain the  $m = 0$  term in (A31), wherein  $\widehat{\Psi}_m$  and  $\kappa_m$  are now  $z$ -independent and  $\widehat{a}_0 = \sqrt{\frac{\pi\bar{c}(0)}{\omega\nu(0)}}$  as discussed after (A33). Alternatively, one has the approximate PB expression of (A16) which is valid, though, only in the “non-dispersive” regime defined in (A34). Setting there  $\omega \approx T^{-1}$  we obtain  $z \ll \frac{2\pi}{\nu_0^2\bar{c}_0T}$ . Subfigures 2(a)–2(c) depict the initial data and snapshots of the numerical solutions for two different propagation times. The time in Fig. 2(b) has been chosen so that the wavepacket is centered about the point  $z_j = j\pi/2\nu_0$  with  $j$  being an odd integer. According to the approximate PB solution of (A16), the waveform at  $z_j$  for odd  $j$  is a Hilbert transform of the initial distribution, whereas, for even  $j$ , the waveform

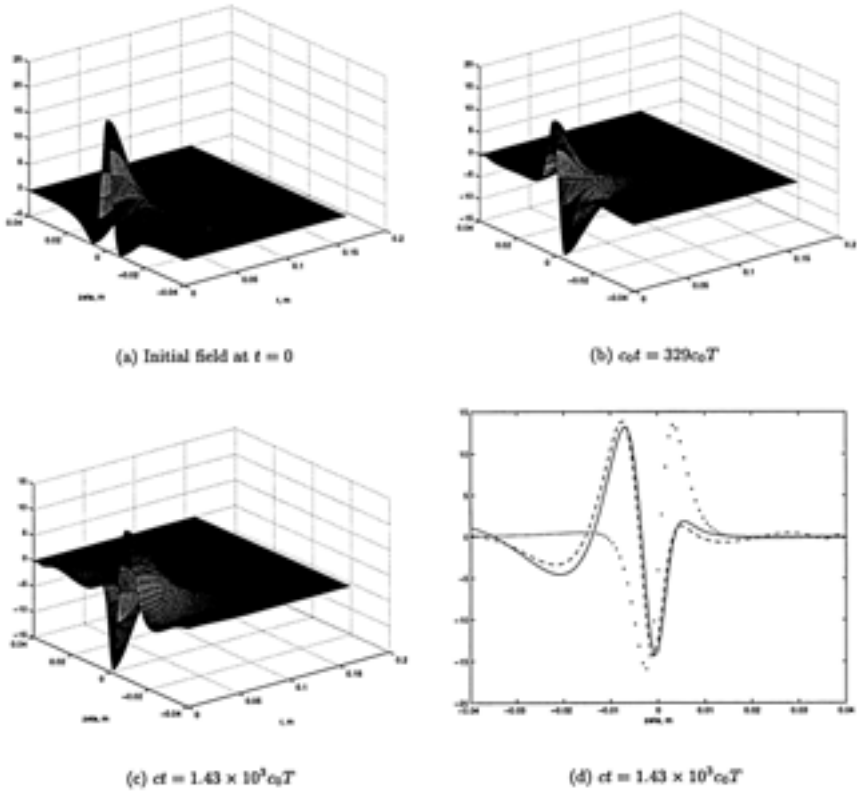


**Figure 2.** Snapshots of the  $p$  field propagating in a quadratic waveguide. The uniform guide is described in (39) with  $c_0 = 1$ ,  $\nu = 7$  and  $a = 0$ . The initial distribution is given in (40) with  $\alpha_0 = i7$  (a matched PB) and with a  $\delta^{\ddagger(2)}$  pulse with  $T = 1.4 \times 10^{-2}$ . The numerical implementation uses  $\Delta\zeta = 2 \times 10^{-4}$ ,  $\Delta_r = 10^{-3}$ ,  $\gamma_\zeta = 0.4$  (i.e.,  $\Delta_t = 5.71 \times 10^{-3}T$ ),  $I = 400$  and  $J = 160$ . The cladding region begins at  $R = J\Delta_r/2$ . The time in (b) was chosen so that the wavepacket is essentially a Hilbert transform of the initial distribution, while (c) is at very late time. In (d) the axial distribution for the numerical solution in (c) or  $r = 0$  is shown versus the corresponding exact and the approximate solutions (note that the numerical solution correctly models the modal dispersion of the exact solution).

is a replica of the initial distribution. Fig. 2(c) is a snapshot of the field at a very long propagation distance ( $10^3$  pulse lengths). Finally, in Fig. 2(d) we compare the axial distributions of the numerical solution shown in Fig. 2(c) with the exact modal solution (transformed numerically to the time domain), and with the approximate PB solution. Note that the numerical solution is very close to the exact solution and that it models correctly the modal dispersion which is quite significant at that distance. One also observes that this modal dispersion is not accounted-for in the nondispersive PB approximation, which breaks down at this large distance.

In Fig. 3 the parameter  $\alpha(0) = i9$  and the PB is *not* matched to the guide. Since the guide is uniform as it was in Fig. 2, the exact solution is now found via a numerical transformation of the modal summation in (A31) into the time domain. The spectra of the mode amplitudes  $\hat{a}_m(\omega)$  in (A31) are specified in (A33). The approximate PB solution for this case is given in (A10) with (A15). As discussed after (A15), the PB solution fluctuates along the guide. Since  $\alpha(0)$  is chosen here to be pure imaginary with  $\text{Im}\alpha(0) > \nu_0/\bar{c}$ , the wavepacket is narrowest at  $z_j = j\pi/2\nu_0$  with even  $j$  and is widest at odd  $j$ . The figure format is the same as in Fig. 2. The observation time in Fig. 3(b) has been chosen so that the wavepacket is centered about  $z_j$  with  $j$  odd; hence, the wavepacket is wider than the initial distribution and is also the Hilbert transform of the initial distribution. Here too one observes a good agreement between the exact modal summation solution and the numerical solution at long observation distances (see Fig. 3(d)).

Finally, in Fig. 4 we consider the nonuniform guide defined in (39) with  $\nu_0 = 7$  and  $\bar{c} = c_0(1 + az)$  with  $\bar{c}_0 = 1$  and  $a = 0.015$ . The initial conditions are given by a non-matched PB with  $\alpha_0 = i9$  so that all modes are excited via (A33). The reference adiabatic mode solution has been calculated via (A31) with the  $\hat{a}_m(\omega)$  specified in (A33). The approximate PB solution in this case is given by (A10) with (A18). One finds that in this case the PB fluctuates along the guide, with quasi-periods defined by  $\int_0^{z_j} \nu(z) dz = 2j\pi$ . Again since  $\text{Im}\alpha(0) > \nu(0)/\bar{c}(0)$  here, one finds that the PB is narrowest at  $z_j$  with even  $j$ , and is widest at odd  $j$ . As in the previous figures the observation time for subfigure 4(b) has been chosen so that the PB is centered about  $z_j$  with odd  $j$ , where the PB is widest and is a Hilbert transform of the initial distribution. Finally, from Fig. 4(d) one observes that the FDTD result agrees with the adiabatic mode

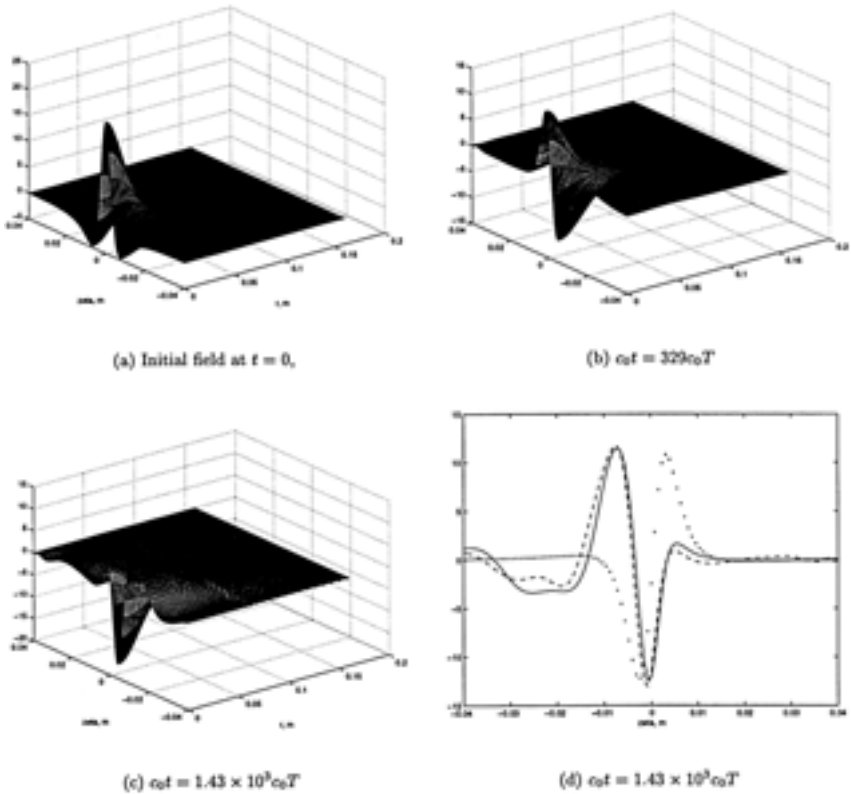


**Figure 3.** Same as in Fig. 2 but for a non matched initial PB distribution with  $\alpha_0 = i9$ .

solution (note that the adiabatic mode approximation again provides a better solution, at large distances, than the approximate PB solution).

#### 4. SUMMARY AND CONCLUSIONS

It has been shown that the modeling of long range propagation of pulsed fields along graded index waveguides is feasible using the moving frame FDTD approach. The distances modeled so far exceed the order of  $10^4$  pulse lengths. The important characteristics of the solution, such as those impacted by physical dispersion phenomena, are reconstructed quite accurately. Obviously, a stationary frame formulation would be impractical for this size of problem. In another

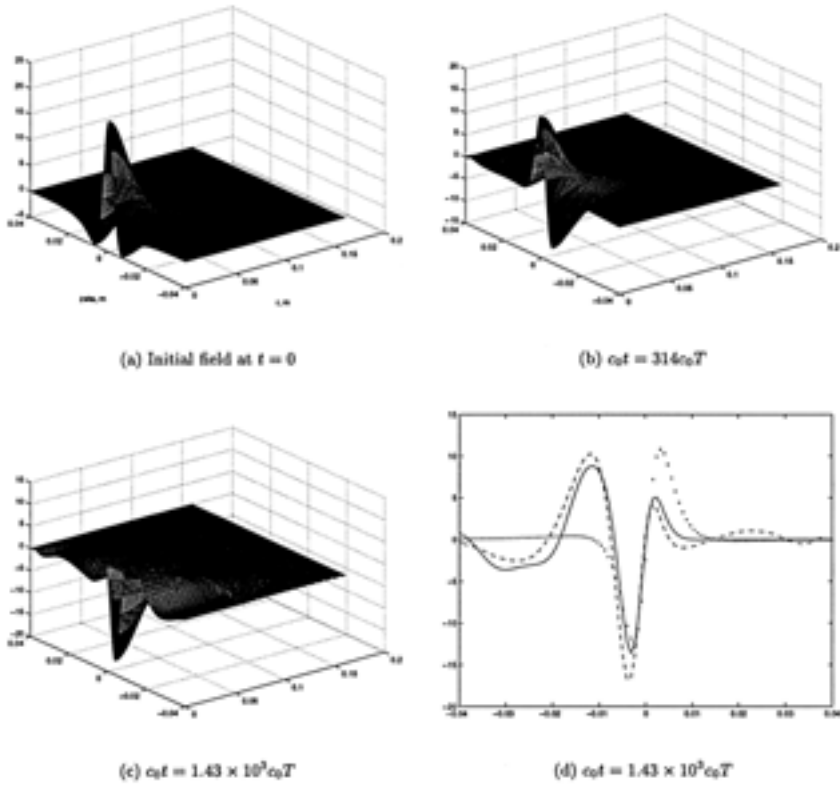


**Figure 4.** Same as in Fig. 2 but for a non uniform guide with  $a = 0.015$  and a non matched initial PB distribution with  $\alpha_0 = i9$ .

paper [7], the propagation of a pulsed beam in non-guiding media such as stratified media is analyzed using a similar technique. For non-guiding environment, the space-time trajectory of the moving frame is also solved for, either by the usage of ray methods or by an automatic numerical technique as suggested in [18]. Initial steps have also been taken towards incorporation of the tools which track pulsed beams along curved trajectories in inhomogeneous media, as was discussed in [7].

In the present case, however, the propagation axis was determined by the guide axis. The moving frame FDTD code for cylindrically symmetric pulsed wave solutions propagating along this axis was given in Sec. 2. In order to account correctly for the physical propagation speed

of the pulsed guided field, the coordinate frame speed was chosen as the local wavespeed along the axis. Based on numerical dispersion and stability expressions, derived in Sections 2.2 and 2.3, respectively, it was shown that the CFL (Courant-Friedrich-Lövy) stability condition for the moving frame FDTD code is governed by the highest possible wavespeed value relative to the frame. For the present case this is the local speed of the backward propagating wave constituents at the side boundary  $r = r_{\max}$  relative to forward propagating frame: The result is the sum of the on-axis speed  $\bar{c}(z)$  and the fastest off-axis speed  $c(r_{\max}, z)$ , see (22).

The absorbing boundary conditions (ABC's) we used in the moving frame FDTD scheme (Section 2.4) are, in essence, adaptations of the first order Engquist-Majda-Mur [14–15] conditions. The ABC's at the front and back boundaries were obtained by transforming the field constituents into adiabatic one-way wave constituents (see (28)) which allowed approximate diagonalizing of the field equations into weakly coupled one-way wave equations. At the back boundary we then removed the incoming (forward propagating) wave constituents from the numerical grid (see (30)), while at the front boundary we set the incoming (backward propagating) wave constituents to zero (see (34)). The difficulty in the formulation of these ABC's was due to the fact that the forward propagating wave constituents were essentially stationary in the moving frame and did not leave it. For the side boundary, it was noted that the propagating field is concentrated in the propagation channel about the axis of the guide, while outside this channel the field is evanescent. Thus, it was shown that the side boundary must be far enough away from the waveguide axis so as to be outside of the propagation channel, even at the lowest end of the frequency spectrum where the channel's width is widest. To annul the non-physical, exponentially growing solutions which are mathematically possible outside of the propagation channel, we set the field constituents to be zero on the side boundary (see (38)).

Finally, the code developed in Section 2 was applied in Section 3 to solve the problem of pulse propagation along waveguiding structures with quadratic profiles. We considered both longitudinally uniform and nonuniform guides. The initial conditions were chosen to give rise to pulsed beam (PB) type solutions [16]. Such PB solutions maintain their wavepacket structure over a considerable distance along the guide. Approximate time domain expressions were developed using

the techniques in [16] and are given in Appendix A.1. These expressions describe the parameters controlling the wavepacket dynamics. For the longitudinally uniform case we also compared the numerical solution with an exact frequency-domain modal solution [17], while for the nonuniform case we developed in Appendix A.2 an adiabatic type modal solution. The numerical solution which was obtained with the moving frame FDTD approach successfully recovers the physical (as opposed to numerical) dispersion characteristics of the modal solution.

## APPENDIX A. WAVEPACKET SOLUTIONS IN GRADED INDEX GUIDES

In this appendix we consider a class of pulsed field solutions in nonuniform graded index waveguides (e.g., optical and dielectric waveguides). We employ the three dimensional coordinate frame  $\mathbf{r} = (x_1, x_2, z)$  where  $z$  is the coordinate along the waveguide axis and  $(x_1, x_2)$  are the transverse coordinates. Within the scalar approximation, the field  $p$  satisfies the time-dependent wave equation

$$\left( \partial_z^2 + \partial_{x_1}^2 + \partial_{x_2}^2 - \frac{1}{c^2(\mathbf{r})} \partial_t^2 \right) p(\mathbf{r}, t) = 0. \quad (\text{A1})$$

The wavespeed  $c(\mathbf{r})$  in the guide has a minimum along the  $z$ -axis, for any constant  $z$ . Since the field is localized within the vicinity of the  $z$  axis, it suffices to expand the transverse variations of  $c$  to second order in  $x_{1,2}$ . Henceforth we shall assume that  $c(\mathbf{r})$  is cylindrically symmetric, although the solution may readily be extended to non-symmetric cases. Under these conditions,  $c(\mathbf{r})$  has the general form in (39) where  $r = \sqrt{x_1^2 + x_2^2}$ ,  $\bar{c}(z)$  is the on-axis wavespeed, and  $\bar{n}(r, z)$  denotes the waveguide profile. Both functions vary slowly with  $z$ .

In Sec. A.1 below we develop closed form approximate expressions which are used to clarify the parameters that control wavepacket dynamics, while in Sec. A.2 we derive the alternative adiabatic mode solution of these wavepackets.

### A.1 Pulsed Beam Solutions in Nonuniform Guide

#### A.1.1 Analytic Signal Representation

The time domain solutions considered here are described in the simplest form by using the analytic signal representation. An analytic

signal  $\overset{+}{p}(t')$ ,  $t' \in \mathbb{C}^-$  corresponding to the real signal  $p(t)$ ,  $t \in \mathbb{R}$  with frequency spectrum  $\widehat{p}(\omega)$ , is defined by the positive frequency inverse Fourier transform

$$\overset{+}{p}(t') = \frac{1}{\pi} \int_0^\infty d\omega e^{-i\omega t'} \widehat{p}(\omega), \quad \text{Im}t' \leq 0 \quad (\text{A2})$$

This integral definition implies that  $\overset{+}{p}$  is an analytic function in the lower half of the complex  $t'$ -plane. It may also be defined *directly* from the *real* signal  $p(t)$  via

$$\overset{+}{p}(t') = \frac{1}{\pi i} \int_{-\infty}^\infty dt \frac{p(t)}{t - t'}, \quad \text{Im}t' \leq 0 \quad (\text{A3})$$

The *real*  $t$  limit of  $\overset{+}{p}(t')$  is thus related to  $p(t)$  via  $\overset{+}{p}(t) = p(t) + i\mathcal{H}p(t)$ , where  $\mathcal{H} = \frac{\mathcal{P}}{\pi t} \otimes$  is a Hilbert transform with  $\otimes$  denoting a convolution and  $\mathcal{P}$  denoting Cauchy's principal value. Thus, if  $\overset{+}{p}(\mathbf{r}, t)$  is an analytic wave solution, then for  $t \in \mathbb{R}$  both  $p_R \equiv \text{Re}\overset{+}{p}$  and  $p_I \equiv \text{Im}\overset{+}{p} = \mathcal{H}p_R$  are *real* wave solutions. We usually consider only  $p_R$ , since  $p_I$  (or any other linear combination of  $p_R$  and  $p_I$ ) may be obtained by multiplying  $\overset{+}{p}$  by a complex constant and taking the real part.

### A.1.2 Wavepacket Solutions

Since the PB is localized in space-time we shall express  $\overset{+}{p}$  in a moving coordinate frame centered about the pulse:

$$\overset{+}{p}(\mathbf{r}, t) = \overset{+}{P}(\mathbf{r}, \tau), \quad \tau = t - \int^z \frac{dz'}{c(z')}. \quad (\text{A4})$$

This coordinate transformation yields  $\partial_z^2 \overset{+}{p} = (\partial_z^2 - \frac{2}{c} \partial_z \partial_\tau + \frac{1}{c^2} \partial_\tau^2 + \frac{c'}{c^2} \partial_\tau) \overset{+}{P}$  where the prime denotes a derivative with respect to  $z$ . Next, it is assumed that pulse length is very short, while the pulse shape is slowly varying function of  $z$ , i.e.,

$$|\partial_z \overset{+}{P}| \ll |c^{-1} \partial_\tau \overset{+}{P}|. \quad (\text{A5})$$

Eq. (A5) implies the approximation  $\partial_z^2 \simeq (-\frac{2}{c} \partial_z \partial_\tau + \frac{1}{c^2} \partial_\tau^2 + \frac{c'}{c^2} \partial_\tau) \overset{+}{P}$ . Defining  $\overset{+}{P} = \sqrt{c} \overset{+}{V}$  and substituting in (A1) with (39), we obtain the

“wavepacket equation” for our quadratic profile case:

$$\left( \partial_{x_1}^2 + \partial_{x_2}^2 - \frac{2}{\bar{c}(z)} \partial_z \partial_\tau + \frac{\nu^2(z)}{\bar{c}^2(z)} r^2 \partial_\tau^2 \right) \overset{+}{V}(\mathbf{r}, \tau) = 0. \quad (\text{A6})$$

It is shown below that (A6) has an exact closed form solution of the form

$$\overset{+}{V}(\mathbf{r}, \tau) = A(z) f^\dagger \left( \tau - \frac{1}{2} r^2 \alpha(z) \right) \quad (\text{A7})$$

where  $f^\dagger(t)$  is an arbitrary analytic signal, which will be assumed to be a short pulse of length  $T$  (e.g., see Sec. A.1.5), while  $A$  and  $\alpha$  are complex functions to be determined.  $\text{Im}\alpha$  controls the PB width. In order to ensure transversal confinement of the solution it is required that  $\text{Im}\alpha(z) > 0$  (see footnote<sup>3</sup> for proof that this condition is satisfied if the initial value is  $\text{Im}\alpha(0) > 0$ ).<sup>2</sup>

Substituting (A7) into (A6), one obtains  $r^2[\alpha'/\bar{c} + \alpha^2 + \nu^2/\bar{c}^2]A f'' - [A\alpha + A'/\bar{c}]f = 0$ . Thus (A7) is a solution for any  $f^\dagger$  if the following  $z$ -dependent ODE's are satisfied:

$$\alpha' + \bar{c}\alpha^2 + \nu^2/\bar{c} = 0 \quad \text{and} \quad A\alpha + A'/\bar{c} = 0 \quad (\text{A8})$$

To solve the first (Riccati-type) equation in (A8) we set  $\alpha(z) = p(z)/q(z)$  and obtain the linear system of first order equations

$$q' = \bar{c}p, \quad p' = -(\nu^2/\bar{c})q \quad (\text{A9})$$

with the initial conditions  $q(0) = 1$  and  $p(0) = \alpha(0)$ . In the most general case this equation will have to be solved numerically. Specific analytic solutions are given in Secs. A.1.3 and A.1.4. Its solution also determines  $A(z)$  via (A8) which yields  $A'/A = -\bar{c}\alpha = -q'/qA(z) = 1/q(z)$ . The final solution is thus given by

$$\overset{+}{p}(\mathbf{r}, t) = \sqrt{\frac{\bar{c}(z)}{\bar{c}(0)}} \frac{1}{q(z)} f^\dagger \left( t - \int_0^z \frac{dz'}{\bar{c}(z')} - \frac{1}{2} \alpha(z) r^2 \right) \quad (\text{A10})$$

This expression is the general solution for a cylindrically symmetric PB in a nonuniform, cylindrically symmetric guide with quadratic profile.

---

<sup>2</sup> For astigmatic solutions,  $r^2\alpha$  is replaced by the quadratic form  $\mathbf{x}^t\alpha\mathbf{x}$  where  $\alpha$  is a  $2 \times 2$  complex symmetric matrix with  $\text{Im}\alpha(z)$  positive definite.

This solution has the characteristics of a pulsed beam, i.e., it is localized both in the axial and transversal directions: Axial confinement around  $z \simeq \bar{c}t$  is provided by the pulse shape of  $f^\dagger$ . Transverse confinement is due to the general property of analytic signals which tend to decay as the imaginary part of their argument becomes more negative (see (A2)). In our case, since  $\text{Im}\alpha(z) > 0$ , (see proof below<sup>3</sup>) the argument of  $f^\dagger$  in (A10) has a negative imaginary part whose magnitude increases quadratically with  $r$ , causing the waveform in (A10) to decay away from the beam axis. The beam is narrow if the decay rate of  $f^\dagger$  in the lower half of the complex plane is high; this can be affected by either (a) a higher frequency content in  $f^\dagger$ , or (b) a larger  $\text{Im}\alpha(z)$  (see a specific example in Sec. A.1.5).

To further quantify the properties of the field we separate the terms in (A10) into real and imaginary parts as follows:

$$\overset{\dagger}{p}(\mathbf{r}, t) = \{A_R(z) + \iota A_I(z)\} f^\dagger[t - t_p(z, r) - \eta(z, r)] \quad (\text{A11})$$

where

$$t_p(z, r) = \int_0^z \frac{dz'}{\bar{c}(z')} + \frac{1}{2}r^2 \text{Re}\alpha(z), \quad (\text{A12a})$$

$$\eta(z, r) = \frac{1}{2}r^2 \text{Im}\alpha(z) > 0. \quad (\text{A12b})$$

Clearly,  $t_p(z, r)$  is the paraxial delay and thus  $(\bar{c}(z)\text{Re}\alpha)^{-1}$  is the wavefront radius of curvature. The transverse decay of the wavepacket is caused by the term  $\eta$ ; as alluded to above, the larger  $\eta$  (or  $\text{Im}\alpha(z)$ ) the weaker the signal and the narrower the beamwidth.

Finally, we discuss the properties of the *real* PB field. It is convenient to introduce the *real* functions  $f_\eta(t)$  and  $\bar{f}_\eta(t) = \mathcal{H}f_\eta(t)$  via (see discussion following (A3))

$$f^\dagger(t - \eta) \equiv f_\eta(t) + \iota \bar{f}_\eta(t) \quad (\text{A13})$$

---

<sup>3</sup> We start with  $\text{Im}\alpha(z) = [\alpha(z) - \alpha^*(z)]/2\iota = [pq^* - p^*q]/2\iota pq^*$ . Noting from Eq. (A9) that  $\frac{d}{dz}[pq^* - p^*q] = 0$  and taking the initial values of  $p$  and  $q$  as specified after (A9), we arrive at  $\text{Im}\alpha(z) = \text{Im}\alpha(0)/qq^*$  which implies that  $\text{Im}\alpha(z) > 0$  provided that  $\text{Im}\alpha(0) > 0$ .

From (A11), the *real* field solution is given by

$$p_R = A_R(z)f_\eta(t - t_p) - A_I\bar{f}_\eta(t - t_p) \quad (\text{A14})$$

where  $\eta$  and  $t_p$  are functions of  $(z, r)$  as defined in (A12). In this formulation, the PB property of transversal confinement is due to the fact that  $f_\eta$  decays with increasing  $\eta$ . Note also that the balance between  $A_R$  and  $A_I$  changes with  $z$ , thereby affecting the relative excitation amplitudes of  $f_\eta$  and  $\bar{f}_\eta$ .

### A.1.3 Special Case I: A Longitudinally Uniform Guide

We consider first the PB solution for the case where  $\bar{c}$  and  $\nu$  are independent of  $z$ , i.e.,  $\bar{c} = \bar{c}_0$  and  $\nu = \nu_0$ . In this case, exact frequency domain modal solutions are available. Their relation to the PB solution is considered in Sec. A.2.3.

For the longitudinally uniform medium, Eq. (A9) takes on the harmonic form  $q'' + \nu_0^2 q = 0$  whose solution for the initial conditions shown after (A9) is

$$q(z) = \cos \nu_0 z + (\bar{c}_0 \alpha(0) / \nu_0) \sin \nu_0 z \quad (\text{A15a})$$

$$\alpha(z) = \alpha(0) \frac{\cos \nu_0 z - (\bar{c}_0 \alpha(0) / \nu_0)^{-1} \sin \nu_0 z}{\cos \nu_0 z + (\bar{c}_0 \alpha(0) / \nu_0) \sin \nu_0 z} \quad (\text{A15b})$$

The final solution is given by (A10) with (A15). Its characteristics have already been discussed after (A10). In the present context we also note from (A15) that the beamwidth fluctuates along the  $z$  axis with period  $2\pi/\nu_0$ . Taking, without loss of generality,  $\alpha(0) = i\bar{\alpha}_0$  to be pure imaginary with  $\bar{\alpha}_0 > 0$  (see discussion in footnote<sup>3</sup>), then  $\text{Im}\alpha(z)$  changes between the two extreme values of  $\bar{\alpha}_0$  and  $\nu_0^2/\bar{c}_0^2\bar{\alpha}_0$ , obtained at  $z_j = \pi j/2\nu_0$ . For the case, say, of  $\bar{\alpha}_0 > \nu_0/\bar{c}_0$ , the wavepacket becomes narrowest or widest at  $z_j$  with even or odd  $j$ , respectively. At these points,  $\text{Re}\alpha = 0$ , i.e., the wavefronts are planar. In the regions between these points,  $\text{Re}\alpha \geq 0$  such that the wavefront diverges or converges as the PB approaches a wide or narrow point, respectively.

An important special case occurs when the PB is *matched* to the guide, i.e., when  $\alpha(0) = \nu_0/\bar{c}_0$ . In this case  $\alpha(z) = \alpha(0)\forall z$  so that the solution in (A10) reduces to

$$\overset{+}{p}(\mathbf{r}, t) = e^{-\nu_0 z} \overset{+}{f}(t - z/\bar{c}_0 - i(\nu_0/2\bar{c}_0)r^2), \quad (\text{A16})$$

i.e., the beamwidth does not fluctuate with  $z$ .

#### A.1.4 Special Case II: A Weakly Nonuniform Guide

In this case we can rewrite (A9) as

$$(q/\sqrt{\bar{c}})'' + (\nu^2 + \bar{c}''/2\bar{c} - 3(\bar{c}')^2/4\bar{c}^2) (q/\sqrt{\bar{c}}) = 0 \quad (\text{A17})$$

Assuming next that  $\nu \gg |\bar{c}'/\bar{c}|$  and solving the resulting equation for  $q/\sqrt{\bar{c}}$  via the WKB approximation yields

$$q(z) = \sqrt{\frac{c(z)\nu(0)}{c(0)\nu(z)}} (\cos \psi(z) + (\bar{c}(0)\alpha(0)/\nu(0)) \sin \psi(z)) \quad (\text{A18a})$$

where  $\psi(z) = \int_0^z \nu(z') dz'$ . Finally, one has

$$\alpha(z) = \alpha(0) \frac{\nu(z)\bar{c}(0)\cos\psi(z) - (\bar{c}(0)\alpha(0)/\nu(0))^{-1}\sin\psi(z)}{\nu(0)\bar{c}(z)\cos\psi(z) + (\bar{c}(0)\alpha(0)/\nu(0))\sin\psi(z)} \quad (\text{A18b})$$

All other properties of the PB are the same as those discussed in the content of the longitudinally uniform guide. Note in particular that the wavefunction is nonuniformly periodic, with quasiperiods defined by the points  $\psi(z) = 2\pi j$ . For the special case of  $\alpha(0) = \nu(0)/\bar{c}(0)$  we find that  $\alpha(z) = \nu(z)/\bar{c}(z)$  giving the matched PB solution of the form (see (A10))

$$\overset{+}{p}(\mathbf{r}, t) = \sqrt{\frac{\nu(z)}{\nu(0)}} e^{-i\psi(z)} f^+ \left( t - \int_0^z \frac{dz'}{\bar{c}(z')} - \frac{\nu(z)r^2}{2\bar{c}(z)} \right) \quad (\text{A19})$$

#### A.1.5 Specific Pulse Shapes: Analytic $\delta$ Pulses

The PB solution may accommodate any analytic pulse shape. As an example, we consider the  $n$ -times differentiated analytic- $\delta$  pulse

$$f^+(t) = \delta^{+(n)} \left( t - i\frac{1}{2}T \right) = (-)^n n! / \pi i \left( t - \frac{1}{2}iT \right)^n, \quad T > 0 \quad (\text{A20})$$

where  $T$  is a measure of the pulse length. The spectrum of these pulses is  $\widehat{f}(w) = (-iw)^n e^{-\omega T/2}$ . The derivatives suppress the low frequencies and thus create a more localized (faster decaying) PB in both the axial and transversal directions. Typically, we use  $n = 2$ , however for simplicity we discuss the PB properties for the case  $n = 0$ .

The real waveforms in (A13) are given by

$$f_{\eta}(t) = \text{Re}\delta^{\dagger}\left(t - i\left(\frac{1}{2}T + \eta\right)\right) = \pi^{-1} \frac{\frac{1}{2}T + \eta}{t^2 + \left(\frac{1}{2}T + \eta\right)^2} \quad (\text{A21a})$$

$$\bar{f}_{\eta}(t) = \text{Im}\delta^{\dagger}\left(t - i\left(\frac{1}{2}T + \eta\right)\right) = -\pi^{-1} \frac{t}{t^2 + \left(\frac{1}{2}T + \eta\right)^2} \quad (\text{A21b})$$

For a given  $\eta$ , the half-amplitude pulse-width in (A21a) is  $(T+2\eta)$  and the peak amplitude is  $\pi^{-1}(\frac{1}{2}T + \eta)^{-1}$ . Thus the waveform is strongest and shortest for  $\eta = 0$  (the beam axis), and decays as  $\eta$  grows away from the axis. The half-amplitude beamwidth is obtained when  $\eta = \frac{1}{2}T$ . Using (A12b), the beam diameter is found to be

$$W(z) = 2\sqrt{T/\text{Im}\alpha(z)} \quad (\text{A22})$$

where  $\alpha(z)$  is the solution of (A8). Using (A22) for the special case of a matched PB where  $\alpha(z) = \nu(0)/\bar{c}(0)$  (see (A16) and (A19)), we obtain the beam diameter at  $z = 0$ :

$$W_0 = 2\sqrt{\bar{c}(0)T/\nu(0)}. \quad (\text{A23})$$

This relation between the pulse length and the beam width may be used as a rule of thumb for the matching condition of any pulsed field excitation. If this condition is not met, then, as discussed in conjunction with (A15), the beamwidth fluctuates as the PB propagates along the guide.

Other pulse types, such as non-modulated or modulated Gaussian pulses, or modulated  $\delta$  pulses, can be treated by the same procedure.

## A.2 Adiabatic Mode Approximation

### A.2.1 Frequency Domain Solutions

As in the previous section, we restrict the discussion to cylindrically symmetric field solutions in cylindrically symmetric guides with

quadratic profile as in (39). In the frequency domain, the field satisfies the wave equation

$$\left( r^{-1} \partial_r r \partial_r + \partial_z^2 + \frac{\omega^2}{\bar{c}^2(z)} (1 - \nu^2(z) r^2) \right) \hat{p}(\mathbf{r}, \omega) = 0 \quad (\text{A24})$$

For any given  $z$ , the transversal eigenfunctions  $\hat{\Psi}_m(r; z)$  are defined by

$$\left( r^{-1} \partial_r r \partial_r + \frac{\omega^2}{\bar{c}^2(z)} (1 - \nu^2(z) r^2) \right) \hat{\Psi}_m = (\omega \kappa_m)^2 \hat{\Psi}_m \quad (\text{A25})$$

The eigenfunctions  $\hat{\Psi}_m$  and eigenvalues  $\kappa_m$  are given by

$$\hat{\Psi}_m(r; z) = \sqrt{\frac{\omega \nu(z)}{\pi \bar{c}(z)}} e^{-\xi/2} L_m(\xi), \quad \xi = \omega \nu(z) r^2 / \bar{c}(z) \quad (\text{A26a})$$

$$\kappa_m(z) = \bar{c}^{-1}(z) \sqrt{1 - 2\nu(z) \bar{c}(z) (2m + 1) / \omega} \quad (\text{A26b})$$

where  $L_m$  are the Laguerre polynomials of order  $m$ . At any given  $z$ , these eigenfunctions satisfy the orthonormality condition

$$\langle \hat{\Psi}_n, \hat{\Psi}_m \rangle \equiv 2\pi \int_0^\infty r dr \hat{\Psi}_m \hat{\Psi}_n = \delta_{m,n} \quad (\text{A27})$$

where  $\delta_{m,n}$  is the Kronecker-function.

Next, we expand the field in the form

$$\hat{p}(\mathbf{r}, \omega) = \sum_m \hat{a}_m \hat{P}_m(z) \hat{\Psi}_m(r; z) \quad (\text{A28})$$

where  $\hat{P}_m(z)$  are amplitude functions, normalized to have  $\hat{P}_m(0) = 1$ , and  $\hat{a}_m$  are determined from the initial conditions

$$\hat{a}_m = 2\pi \int_0^\infty r dr \hat{\Psi}_m \hat{p}|_{z=0} \quad (\text{A29})$$

Substituting (A28) into (A24) using, and then projecting the result on  $\hat{\Psi}_n$  using (A27), one obtains

$$(\partial_z^2 + \kappa_n^2(z)) \hat{P}_n + \sum_m \langle \hat{\Psi}_n, \partial_z^2 \hat{\Psi}_m \rangle (\hat{a}_m / \hat{a}_n) \hat{P}_m = 0 \quad (\text{A30})$$

The first term on the left is the wave operator for the modal amplitude. Since the  $\widehat{\Psi}_n$ 's are slowly varying functions of  $z$ , the summation which represents mode coupling due to the  $z$  variations will be neglected. Note also that typically  $\widehat{a}_m/\widehat{a}_n \rightarrow 0$  as  $m \rightarrow \infty$ . The resultant equation may then be solved by an adiabatic (WKB-type) approximation, giving the final solution

$$\widehat{p}(z, r; \omega) = \sum_m \widehat{a}_m(\omega) \widehat{\Psi}_m(r; z) \sqrt{\frac{\kappa_m(0)}{\kappa_m(z)}} e^{i\omega \int_0^z \kappa_m(z') dz'} \quad (\text{A31})$$

Finally, the time-domain field is obtained by transforming this expression into the time domain. Note in particular that the solution in (A31) is exact for a longitudinally uniform guide.

### A.2.2 Modal Amplitudes for the PB Excitation

For a PB excitation (A10), the coefficients  $\widehat{a}_m$  in (A29) can be found in closed form. We first note that the frequency domain counterpart of the initial field distribution of the PB in (A10) is given by

$$\widehat{p}(0, r; \omega) = \widehat{f}(\omega) e^{i\omega\alpha(0)r^2/2} \quad (\text{A32})$$

where  $\widehat{f}$  is the frequency spectrum of the analytic pulse  $f^+$ . Substituting in (A32) in (A29), and using the identity  $\int_0^\infty d\xi e^{-\eta\xi} L_m(\xi) = (\eta - 1)^n \eta^{-m-1}$ , one obtains

$$\widehat{a}_m(\omega) = (-)^m \sqrt{\frac{4\pi\bar{c}(0)}{\omega\nu(0)}} \frac{(1 + i\alpha(0)\bar{c}(0)/\nu(0))^m}{(1 - i\alpha(0)\bar{c}(0)/\nu(0))^{m+1}} \quad (\text{A33})$$

Note in particular that under the matched PB conditions  $\alpha(0) = \nu(0)/\bar{c}(0)$  (see (A19)),  $\widehat{a}_m = 0$  for  $m \geq 1$ , while  $\widehat{a}_0 = \sqrt{\frac{\pi\bar{c}(0)}{\omega\nu(0)}}$ . Thus *the matched PB is in fact a wide band solution tuned to excite only the  $m = 0$  mode at all frequencies.*

### A.2.3 The Non-dispersive PB Approximation

In general, the mode series cannot be transformed into the time domain analytically. For high frequency excitations, however, the series

may be summed in closed form and transformed into the time domain. We start by approximating (A26b) in a Taylor series

$$\kappa_m \approx 1/\bar{c}(z) - \nu(z)(2m+1)/\omega \quad (\text{A34})$$

This approximation may be used as long as the phase error introduced by the next order term is negligible. For the  $m$ th mode, this condition is

$$\int_0^z dz' \frac{1}{2} \bar{c}(z') \nu^2(z') (2m+1)^2 \omega^{-1} \ll \pi \quad (\text{A35})$$

Next, we substitute (A34) into the expressions for the modal phases, while for the amplitudes we use only the first order term. The  $m$ th term in the series (A31) now becomes

$$\hat{f}(\omega) \hat{a}_m(\omega) \sqrt{\frac{\bar{c}(z)}{\bar{c}(0)}} \hat{\Psi}_m(r, z) e^{i\omega \int_0^z \frac{dz'}{\bar{c}(z')}} e^{-i(2m+1) \int_0^z \nu(z') dz'}. \quad (\text{A36})$$

Using  $\hat{a}_n$  from (A33) and the standard expansion of  $e^{-\eta\xi}$

$$e^{-\eta\xi} = \sum_{m=0}^{\infty} \left(\eta - \frac{1}{2}\right)^m \left(\eta + \frac{1}{2}\right)^{-m-1} e^{-\xi/2} L_m(\xi) \quad (\text{A37})$$

the  $m$ -series may be summed in closed form, giving

$$\hat{p}(\mathbf{r}, \omega) = \hat{f}(\omega) \sqrt{\frac{\bar{c}(z)}{\bar{c}(0)}} \frac{1}{q(z)} e^{i\omega \int_0^z \frac{dz'}{\bar{c}(z')} + i\omega \frac{1}{2} \alpha(z) r^2} \quad (\text{A38})$$

where  $\alpha(z)$  and  $q(z)$  are given in (A18). This expression is readily recognized as the frequency domain counterpart of (A10). As a special case, one should note that the matched PB solution in (A16) is the time domain counterpart of the  $m=0$  mode under the high frequency approximation in (A34).

This analysis establishes the PB solution in Section A.1 as a non-dispersive approximation of the modal solution (A31). Essential in this identity is the requirement that the *mode amplitude spectra* should be prescribed by (A33), i.e., the PB blends the wide spectrum superposition of modes in such a way that the time domain solution retains its wavepacket structure throughout the non-dispersive propagation regime defined by (A35).

## REFERENCES

1. Yee, K. S., "Numerical solution of initial boundary value problems involving Maxwell's equations in isotropic media," *IEEE Trans. Antennas Propagat.*, Vol. AP-14, 302–307, 1966.
2. Taflov, A., *Computational Electrodynamics, The Finite-Difference Time-Domain Method*, Artech House, Boston, 1995.
3. Shlager, K. L., and J. B. Schneider, "A selective survey of the finite-difference time-domain literature," *IEEE Antennas Propagat. Magazine*, Vol. 37, No. 4, 39–56, 1995.
4. Fidel, B., E. Heyman, R. Kastner, and R. W. Ziolkowski, "Hybrid ray-FDTD moving window approach to pulse propagation," *Proc. of the 1994 International IEEE/AP-S Symposium*, Seattle, WA, 1414–1417.
5. Fidel, B., E. Heyman, R. Kastner, and R. W. Ziolkowski, "Hybrid ray-FDTD moving frame approach to pulse propagation," *J. of Comp. Phys.*, Vol. 138, 480–500, 1997.
6. Hile, C. V., and W. L. Kath, "Numerical solutions of Maxwell's equations for nonlinear-optical pulse propagation," *J. Opt. Soc. Am. B*, Vol. 13, No. 6, 1135–1145, 1996.
7. Pemper, Y., E. Heyman, R. Kastner, and R. W. Ziolkowski "Hybrid ray-FDTD moving coordinate frame approach for long range tracking of collimated wavepackets," *SIAM J. Appl. Math.*, submitted.
8. Lee, D., and A. D. Pierce, "Parabolic equation development in recent decade," *J. Comput. Acoust.*, Vol. 3, No. 2, 95–173, 1995.
9. Jensen, F. B., W. A. Kuperman, M. B. Porter, and H. Schmidt, *Computational Ocean Acoustics*, AIP Press, Woodbury, NY, 1994.
10. Masoudi, H. M., and J. M. Arnold, "Parallel beam propagation methods," *IEEE Photon. Technol. Lett.*, Vol. 6, No. 7, 848–850, 1994.
11. Murphy, J. E., "Finite-difference treatment of a time-domain parabolic equation: Theory," *J. Acoust. Soc. Am.*, Vol. 77, No. 5, 1406–1417, 1985.
12. Masoudi, H. M., and J. M. Arnold, "Parallel beam propagation method for the analysis of second harmonic generation," *IEEE Photon. Technol. Lett.*, Vol. 7, No. 4, 400–402, 1995.
13. McDonald, B. E., and W. A. Kuperman, "Time domain formulation for pulse propagation including nonlinear behavior at a caustic," *J. Acoust. Soc. Am.*, Vol. 81, No. 5, 1406–1417, 1987.
14. Engquist, B., and A. Majda, "Absorbing boundary conditions for the numerical simulation of waves," *Mathematics of Computation*, Vol. 31, 629–651, 1977.

15. Mur, G., "Absorbing boundary conditions for the finite-difference approximation of the time-domain electromagnetic-field equations," *IEEE Trans. Electromagnetic Compatibility*, Vol. 23, 377–382, 1989.
16. Heyman, E., "Pulsed beam propagation in an inhomogeneous medium," *IEEE Trans. Antennas Propagat.*, Vol. AP-42, 311–319, 1994.
17. Yariv, A., *Introduction to Optical Electronics*, Holt, Rinehart and Winston, 1971.
18. Aloni, E., R. Kastner, E. Heyman, and R. W. Ziolkowski, "Reduction of numerical dispersion errors in the FDTD with multiple moving coordinate systems," URSI Meeting, Baltimore, MD, July 21–26, 1996.